ELSEVIER

Nuclear Instruments and Methods in Physics Research B 193 (2002) 705–712

NIM B
Beam Interactions with Materials & Atoms

www.elsevier.com/locate/nimb

Si-Auger electrons from the center of nuclear tracks

G. Schiwietz [a,*], K. Czerski [a], M. Roth [a], F. Staufenbiel [a], E. Luderer [a], P.L. Grande [b]

[a] *Hahn–Meitner-Institut Berlin GmbH, Strukturforschung SF4, Bereich Festkörperphysik, Glienicker Str. 100, 14109 Berlin, Germany*
[b] *Instituto de Física, Universidade Federal do Rio Grande do Sul, 91500 Porto Alegre, Brazil*

Abstract

Using a new ultra-high vacuum system we were able to measure ion-induced Auger electron spectra with high resolution for atomically clean amorphous Si surfaces. Measurements were performed with Ne^{9+} and Ar^{16+} ions at 5 MeV/u, Xe^{15+} and Xe^{31+} ions at 1.78 MeV/u as well as with incident electron at the two speeds, corresponding to 2.7 keV respectively 1.0 keV. The ion-induced spectra show peaks due to multiple ionization, indicating 7- or 8-fold ionization in the center of ion tracks for fast Xe ions. The Auger peaks are shifted and broadened with respect to the electron reference data. This is an indication for the nuclear-track potential and for hot electrons being present during the decay of the Auger states. © 2002 Published by Elsevier Science B.V.

1. Introduction

The high electronic energy loss of fast heavy ions leads to various modification effects in solids [1–4] and different explanations for the basic track-production mechanisms have been proposed. The corresponding scenarios are *Coulomb explosion* due to the mutual repulsion of ionized target atoms [1], spontaneous lattice relaxation due to *long-lived repulsive states* [5] and the thermal spike due to *electron–phonon coupling* [6] or individual *ion–electron collisions* [7]. These mechanisms may finally yield an unordered atomic motion and if a critical local lattice temperature is exceeded, permanent atomic rearrangement may result on a time scale of 0.1–10 ps. Currently, the pathways of the electronic energy dissipation and the coupling between electronic and atomic degrees of freedom are largely unknown. Thus, for a better understanding of the basic mechanisms, a sound knowledge on the short-time evolution of the nuclear track is necessary.

In previous investigations of convoy electrons and Auger electrons, we could distinguish between the appearance of a nuclear-track potential in polypropylene and mylar [8–11], related to Coulomb explosion, and high electron temperatures pointing to the thermal-spike mechanism in graphite as well as in graphite-like amorphous carbon. The nuclear track potential, resulting from ionization and charge separation in the ion track, leads to decelerated convoy electrons [10,11] and Auger electrons [8,9,11]. The corresponding positive potential attracts electrons and repels positively charged light target ions [12].

Contrary to the two polymers, for semiconductors (graphite and amorphous carbon) no

* Corresponding author. Tel.: +49-30-8062-24-48; fax: +49-30-8062-22-93.
E-mail address: schiwietz@hmi.de (G. Schiwietz).

0168-583X/02/$ - see front matter © 2002 Published by Elsevier Science B.V.
PII: S0168-583X(02)00891-1

indications of a nuclear-track potential could be found. Instead, the Auger structures for these materials show a broadening that increases with increasing projectile charge. This broadening could directly be related to the electron temperature during the Auger decay at the center of the track [11,13]. Recently, similar results have been obtained by Caron et al. for amorphous C at higher ion velocities [14].

Thus, some insulators behave completely different from semi-metals or metals. Therefore, the question arises what is the importance of neutralization and heat conduction inside ion track in semiconductors. In this paper, some first and preliminary answers to this question will be given. Si Auger-electron spectra taken with a new ultra-high vacuum setup will be presented. After an explanation of the setup and the experimental methods, electron- and ion-induced Si-Auger spectra and a first analysis of the data are presented.

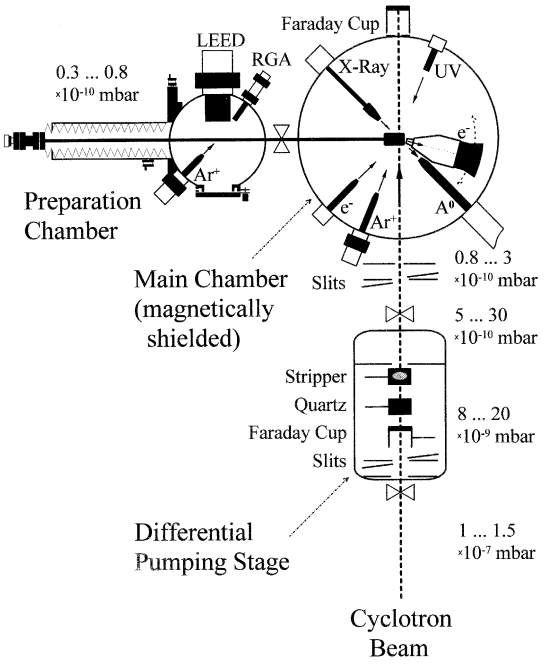

Fig. 1. Experimental setup consisting of three vacuum chambers. The most important attached devices are indicated in the scheme and discussed in the text.

2. Experimental method

The experiments have been performed with fast highly charged particles at velocities of 6–10% the speed of light (at 1.78 and 5 MeV/u) delivered by the heavy-ion cyclotron of the Ionenstrahl-Labor (ISL) at the Hahn–Meitner-Institut Berlin. The setup is described in the following and a scheme of the target station is displayed in Fig. 1.

The setup consists of three different vacuum systems. A double differential pumping stage reduces the pressure from typical values of 10^{-7} mbar in the cyclotron beam line down to about 10^{-10} mbar in the main chamber. Two four-jaw slits systems are used to collimate about 50% of the beam intensity (100–300 nA) to a spot size of 2 mm. A stripper foil (approximately 100 μg/cm^2 C) inside the differential pumping stage allows to switch rapidly to a beam with a quasi-equilibrium charge-state distribution. In the present investigation, this method was used for 5 MeV/u Ne^{9+} and Ar^{16+} and 1.78 MeV/u Xe^{31+} ions. These ion charge states have been interpolated using the casp computer code [15]. In the case of Xe^{31+} a direct determination of the charge-state distribution has also been performed using a dipole magnet after the cyclotron and a similar stripper foil (55 μg/cm^2 Al). The interpolation result of $q_{\mathrm{mean}} = 30.75$ [15] is in good agreement with the experimental result of 30.86 ± 0.08. The use of equilibrium charge-state distributions has the advantage that there is no significant depth dependence of the electronic target excitations.

The preparation chamber is used to exchange targets and to clean and analyze the sample surfaces. Target heating up to a several hundred °C may be performed and the desorption of surface atoms may be monitored using a residual-gas analyzer. An Ar sputter ion gun is used to clean the targets. Ten to 30 min of Ar sputtering do usually yield an atomically clean surface. A new sample is etched chemically prior to mounting on the manipulator and the following initial Ar sputtering lasts for about 10 h. The surface crystal structure may be analyzed in this chamber using the low-energy electron-diffraction technique (LEED). A computer-controlled manipulator allows for all three translational motions as well as for a rota-

tion around the manipulator axis (φ-rotation) and a tilt of the sample (Θ-rotation). After the preparation procedures, the z-motion of this manipulator is also used to reach the sample position inside the main chamber.

The main chamber as displayed in Fig. 1 is equipped with four particle and radiation sources and with two particle analyzers. The X-ray, UV and Ar-ion sources as well as the energy-dispersive neutral-atom analyzer of the main chamber are not used in the present investigation and shall not be mentioned furthermore. The chamber consists of a 2-fold magnetic shielding to reduce the earth magnetic field by factors between 110 at the boundary and 170 at the center of the chamber. This low magnetic field is necessary for angle- and energy-dispersive measurements of low-energy electrons. The electron spectrometer is an electrostatic 45° parallel-plate system with an energy resolution of about 1.7% in the present investigation. Electron intensities are measured in the pulse counting mode using a micro-sphere plate detector. The spectrometer may be rotated around the center of the main chamber. In this work, spectra were taken for a detection angle of 135° with respect to the incident beam, corresponding to 45° with respect to the surface normal. As has been shown in a previous work [16], Auger electrons ejected in backward directions (135°) are induced directly by the projectile (in the central track region). A remaining fraction of about 20% is related to δ-electron cascades in Si.

During the experiments, the ion beam is focused at the center of the chamber with a precision of about 0.3 mm for the central beam spot position. The same precision is reached for the beam from the electron gun. The electron beam-spot size is about 1 mm for target currents of 10 μA. Thus, the electron beam is used to test the sample at the center of the ion irradiated spot.

Boron doped ($<1\ \Omega$cm) Si$\langle 1\,1\,1\rangle$ samples have been used. After sample heating, a 7×7 reconstruction was observed using LEED. In this work we present results for amorphized Si samples. The amorphization was performed using 5 keV Ar^+ ions from the sputter gun. After a few minutes no LEED spot could be observed anymore. Furthermore, it was verified that there is no crystallization due to the irradiation with the fast heavy ion beam.

Pumping in the main chamber is performed with a magnetic and standard turbo-molecular pump in series connected to a diaphragm pump. A liquid nitrogen cooled Ti-sublimation pump is also used during the cyclotron experiments. Since the residual gas in the chamber is dominated by H_2 (typically followed by CO and then H_2O), experiments can last for several hours before the next sputtering cycle of the sample is needed. The surface composition was monitored using electron-induced Auger spectra. It turned out that the relative peak height of the Si-LVV Auger line drops when surface contaminations of any type are present. We estimate that the all-over contamination of the Si surface is below 3% for the sum of all heavier elements (C, O, ...). Ion- and electron-induced electron spectra obtained with these atomically clean Si surfaces are presented and analyzed in the next section.

3. Spectra and data evaluation

Fig. 2 displays an electron spectrum for 2.7 keV electrons incident on amorphous Si. For reference purposes, the electron spectra are taken at the same speed as the incident ions. The measured intensity as shown in the graph is proportional to the doubly differential electron yield $d^2Y/d\Omega\,dE$ times the detected electron energy E_e, since the electron energy resolution is energy dependent corresponding to $\Delta E = 0.017E_e$. Primary electrons hit the target surface under an angle of 45° with respect to the surface normal (see Fig. 1) and the electron detection angle is the same as in the ion experiments (45° with respect to the surface normal and 90° with respect to the electron beam). It is noted that the data in Fig. 2 represent an average of several individual spectra obtained during the Ar^{16+}-ion experiment. Typically two electron spectra have been taken directly after sputter cleaning of the sample and two spectra after each experimental run (including 4–10 spectra) with fast ions. This method has some advantages. We always have well-controlled surface conditions during the ion experiments and the electron reference

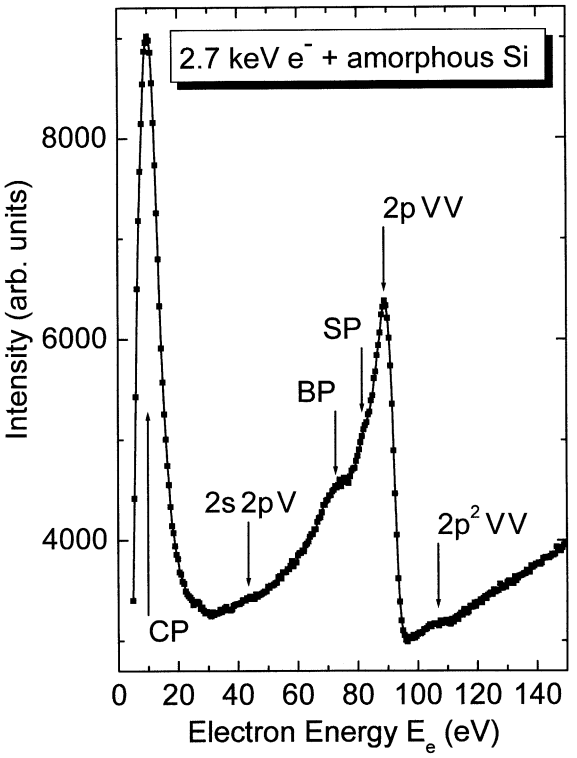

Fig. 2. Electron-energy spectrum for incident electrons on Si. Three Auger structures, the cascade peak (CP), a bulk and a surface plasmon energy-loss peak (BP and SP) are indicated in the plot.

spectra are taken under exactly the same conditions as the ion-induced electron spectra. Comparison of such electron spectra taken with three different Si samples during four beam times within one year indicate an uncertainty of $\Delta E = \pm 0.15$ eV for the electron energy scale.

The electron-energy spectrum in Fig. 2 shows several structures superimposed on a continuous background due to decelerated projectile electrons and secondary electrons. This continuous contribution extends below the Auger peak structures and merges into the so-called cascade peak (CP) at energies around 10 eV. These low-energy electron are most sensitive even to small magnetic or electric fields, as they result, e.g. from surface potential differences in the surrounding of the sample holder. Consequently, we find the largest intensity variations of $\pm 15\%$ (over several months and for different sample holders) for the cascade peak.

Three Auger structures, 2pVV, $2p^2$VV and 2s2pV, are visible in all electron spectra. The dominant Auger peak 2pVV is due to single ionization of the 2p subshell of Si. One valence electron (V) fills the vacant 2p level and transfers the energy to another valence electron (V) which then is ejected. The 2pVV structure is accompanied by two electron-energy loss peaks due to collective excitations. These bulk and surface plasmon peaks (BP and SP) are about 17 and 10 eV below the main peak, respectively. The $2p^2$VV Auger peak at about 103 eV is due to double ionization of the 2p shell, as attributed already in a pioneering work by Schmidt et al. [17]. Only two valence electrons take actively part in this Auger decay, but the reduced screening inside the 2p shell shifts the peak energy in comparison with the 2pVV transition by about 14 eV. The 2s2pV structure at about 44 eV is barely visible in this plot, but it appears in all electron-induced spectra. Here, a 2s vacancy is filled by a 2p or valence-band electron and the other active electron is ejected. A possible 2sVV decay of the 2s vacancy was never observed by us. This indicates that the 2s2pV transition rate exceeds the one for the 2sVV transition by at least a factor of 15, consistent with tabulated Auger coefficients [18].

Fig. 3 displays normalized Si $2p^n$VV Auger-electron structures for 5 MeV/u Ar^{16+} ions and projectile electrons of equal velocity on amorphous Si. The electron data are obtained from the spectrum in Fig. 2. Subtraction of a continuous background and iterative separation of the contributions for single, double and triple L-shell ionization has been performed with the datasets. A multi-parameter fit function was used for the determination of the background. Three fit parameters were determined from the slope of the spectra at energies above the $2p^n$VV structures. After multiplicative adjustment of the fit function to the data in the energy range between 50 and 60 eV, three other fit parameters are optimized. They were used to fit the low-energy part of the spectrum to properly account for the continuous distribution of secondary electrons and the corresponding cascade-electron contribution. With this procedure, the residual Auger spectra, as displayed in the graph, include also the corresponding

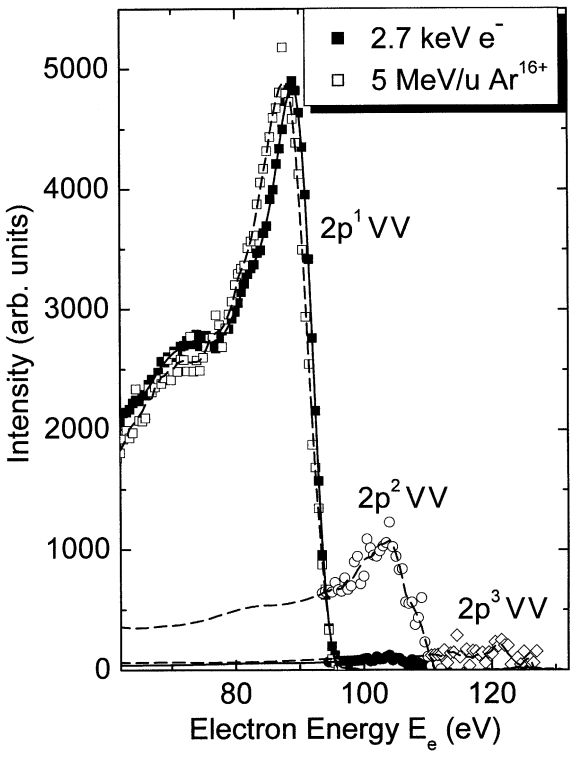

Fig. 3. Si Auger-electron structures for incident electrons and Ar ions after background subtraction and iterative separation of the contributions for different degrees of L-shell ionization.

Auger-electron-induced cascade structure. With minor changes of the parameters we could fit all electron- and ion-induced spectra. At energies below the plasmon shoulder, the background subtracted spectra are independent of the primary particle. Those electrons have suffered a few inelastic collisions far from the particle path and therefore should be independent on the projectile species. This confirms the fitting procedure. It is emphasized that these spectra close to the Auger peak maximum are very insensitive to the details of the subtracted background (even a linear background, if adjusted carefully, gives reasonable results in most cases).

The separation of the $2p^n VV$ Auger structures, as shown in Fig. 3, is based on the assumption that the different peaks may roughly be transformed into each other by applying a linear scaling of the energy axis and intensity. Although such a scaling should not be valid for structures in the electron energy-loss distribution, the general trends should be well described. In a first step, a copy of the spectrum is reduced in intensity and the energy axis is stretched by about 15% to fit the $2p^2VV$ peak. The difference of the original spectrum and the copy gives than a first estimate of the $2p^1VV$ peak. Afterwards, the resulting peak spectrum is fitted to the highest $2p^nVV$ Auger structure and subtracted from the original spectrum. The difference is treated in the same way until all Auger components are separated. Further iterations do not improve the quality of the separation for the spectra analyzed in this work.

From the figure it is seen that the spectral intensities as well as the line positions depend significantly on the type of projectile. These two parameters as well as the line width have been extracted from the spectra for the different projectiles and will be discussed in the next section.

4. Results and discussion

Fig. 4 displays the three Auger peak parameters extracted from ion- and electron-induced spectra as, e.g. shown in Fig. 2. The quantities in Fig. 4 are plotted as a function of the electronic perturbation parameter or interaction strength $P = |q_{\mathrm{eff}}|/v_{\mathrm{p}}$, as it appears in quantum mechanical matrix elements for localized excitations, for ionization as well as plasmon production. The projectile velocity in atomic units is denoted v_{p}, and the effective charge q_{eff} is set equal to the mean particle charge state for electrons and the lighter ions. For 1.78 MeV/u Xe^{15+} ($q_{\mathrm{eff}} = 22$) and Xe^{31+} ($q_{\mathrm{eff}} = 32$) ions we have performed rough estimates considering the corresponding shell radii of the projectile shells and the target 2p shell. The error bars in this plot indicate all-over estimates of the uncertainty for each data point.

In Fig. 4(a) relative yields Y_n are given for $2p^nVV$ Auger ejection due to multiple ionization of the Si-2p subshell. These yields are given by the integrated Auger intensities for $2p^nVV$ divided by the sum over all $2p^iVV$ transitions. Energy integrations have been performed with a lower energy limit equal to 50% of the Auger peak energy. Corrections for Auger cascades (a singly ionized

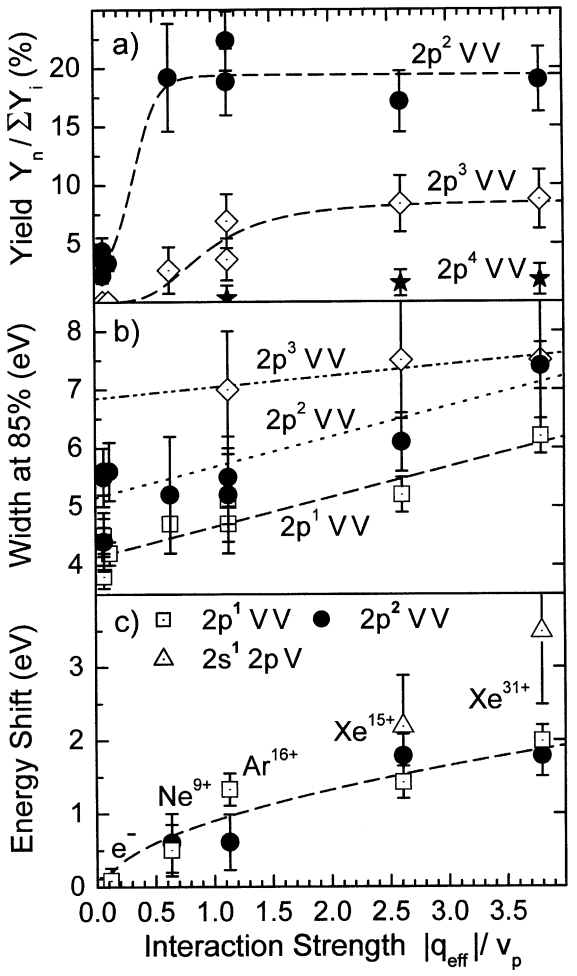

Fig. 4. Auger peak parameters as a function of the perturbation parameter $q_{\mathrm{eff}}/v_{\mathrm{p}}$. (a) Fractional multiple ionization yield; (b) peak width and (c) Auger peak-energy shift.

2p-shell follows each $2p^2VV$ decay) [9,16], for the energy dependent mean free electron path and for δ-electron cascades (fast δ-electrons may produce about 20% single 2p vacancies at the sample surface) [16] have not been applied. The dashed lines are results of least-squares fits, guided by theory [11,19]. The curves for $2p^nVV$ are proportional to P^{2n-2} for small values of the perturbation parameter P (perturbation limit of the independent electron model) and for large values of P they reach a saturation value. An exception is the curve for $2p^2VV$ transitions, where the additional offset value of 3% at $P = 0$ is assigned to shake-off processes. Saturation for n-fold ionization indicates the minimum degree of inner-shell ionization at the center of the track as follows from theory [11]. Considering the four valence-band electrons which are much easier to ionize, saturation of the relative $2p^3VV$ or $2p^4VV$ intensity is a strong hint for 7- or even 8-fold ionization in the center of the ion tracks in Si. Thus, there is a high degree of ionization directly after the interaction of the projectile with the target-electron system.

In Fig. 4(b) the full width at 85% of the peak height is displayed for the $2p^nVV$ Auger peaks (for $n = 1 \ldots 3$). The usual 50% value (full width at half maximum) would not be accurate enough for the present spectra with strongly overlapping Auger structures. The width of the Auger lines increases roughly linear with P and the peak broadening reaches about 2 eV for $P = 3.8$. To within the experimental uncertainty, the slope of the fit curves is identical for the three Auger structures, pointing to a common reason for the broadening of the Auger lines due to an increased perturbation by the projectile. In previous investigations of graphite and graphite-like amorphous carbon, such a broadening could be related to the electron temperature inside ion tracks which influences the structure of the Auger peak [11,13,14]. A quantitative determination of electron temperatures requires a more refined analysis, but even the interpretation is not so clear for the present case as will become obvious in the subsequent discussion.

In Fig. 4(c) the energy shift of ion-induced Auger lines relative to the corresponding electron-induced spectra is displayed. The peak shifts increase monotonically with the interaction strength P and reach about 2 eV for $P = 3.8$. As can be seen from Fig. 3, the ion-induced spectra are shifted towards lower energies. Macroscopic charging of the B-doped Si sample can be excluded, since no indication of a peak shift could be found for incident electrons at different beam currents. Thus, we attribute the measured shift in Fig. 4(c) to the nuclear-track potential induced by the positive charges due to ionization in the center of the track. Auger electrons are decelerated when they leave such a charged region.

From our previous measurements of this effect for polypropylene and mylar [8,9], we estimate

that the initial track potential directly after the interaction with the projectile will be about 200 V for Xe^{31+} ions. Thus, the measured shift of only 2 eV is strongly influenced by the time dependent electronic neutralization of the track. A time dependent potential, however, may also lead to a broadening of the Auger structures as shown in Fig. 4(b). Therefore, we take the present results as evidence for nuclear-track potentials in Si, but the determination of the electronic heat inside tracks awaits detailed simulations of the spectral shape of the Auger peaks.

Note that the first investigation of electron- and ion-induced Si-L Auger spectra by Schmidt et al. [17] has focussed on multiple ionization and no line shifts or broadenings have been reported. In a subsequent work by Koyama et al. [20], both a line shift and a broadening have been observed for a very small incident angle with respect to the target surface. This finding can be related to an enhanced neutralization time due to electrons escaping from the surface or due to the influence of surface states on the neutralization mechanisms. Thus, to our knowledge the present work is the first one to determine this charge-state effect for normal incidence conditions.

5. Conclusions

In this work we have presented a new ultra-high vacuum system for investigations of atomically clean targets. Auger measurements with excellent reproducibility have been performed for electrons, Ne^{9+} and Ar^{16+} ions at 5 MeV/u and with 230 MeV $^{129}Xe^{15+}$ and $^{129}Xe^{31+}$ ions. The analysis allows to distinguish spectra due to multiple ionization of the Si-2p subshell. The saturation of the intensity ratios shows that there is at least 7-fold ionization in the center of the ion tracks, directly after the interaction with Xe projectiles.

A preliminary analysis of the Auger peak positions and widths has revealed an interesting result. For the first time, a material has been investigated that shows a peak-energy reduction as well as also a peak broadening for ions at normal incidence. Both effects increase with the projectile charge. The increasing shift points to a nuclear-track potential. The increasing width, however, is an indication of a hot electronic system, but it may also be influenced by the nuclear-track potential decaying with time. Thus, a refined analysis is necessary to separate both effects and to derive quantitative results for the mean excitation energy inside ion track of Si.

Acknowledgements

We are indebted to M. Rösler for helpful discussions. We also acknowledge the support of one of the authors (P.L.G.) by the Alexander-von-Humboldt foundation and by the PROBRAL contract between the DAAD and Capes.

References

[1] R.L. Fleischer, P.B. Price, R.M. Walker, Nuclear Tracks in Solids, University of California Press, Berkely, CA, 1975.
[2] R. Spohr, Ion tracks and microtechnology, F. Vieweg und Sohn Verlagsge-sellschaft, Braunschweig, 1990.
[3] J. Liu, C. Trautmann, C. Müller, R. Neumann, Nucl. Instr. and Meth. B 193 (2002) 259.
[4] S. Klaumünzer, Ming-dong Hou, G. Schumacher, Phys. Rev. Lett. 57 (1986) 850.
[5] P. Stampfli, K.H. Bennemann, Phys. Rev. B 49 (1994) 7299;
P. Stampfli, Nucl. Instr. and Meth. B 107 (1996) 138.
[6] Z.G. Wang, C. Dufour, E. Paumier, M. Toulemonde, J. Phys.: Condens. Matter 6 (1994) 6733.
[7] A.E. Volkov, V.A. Borodin, Nucl. Instr. and Meth. B 107 (1996) 172.
[8] G. Schiwietz, P.L. Grande, B. Skogvall, J.P. Biersack, R. Köhrbrück, K. Sommer, A. Schmoldt, P. Goppelt, I. Kádár, S. Ricz, U. Stettner, Phys. Rev. Lett. 69 (1992) 628.
[9] G. Schiwietz, G. Xiao, Nucl. Instr. and Meth. B 107 (1996) 113.
[10] G. Xiao, G. Schiwietz, P.L. Grande, A. Schmoldt, N. Stolterfoht, M. Grether, R. Köhrbrück, A. Spieler, U. Stettner, Phys. Rev. Lett. 79 (1997) 1821.
[11] G. Schiwietz, E. Luderer, G. Xiao, P.L. Grande, Nucl. Instr. and Meth. B 175–177 (2001) 1.
[12] K. Wien, Ch. Koch, Nguyen van Tan, Nucl. Instr. and Meth. B 100 (1995) 322.
[13] G. Schiwietz, G. Xiao, P.L. Grande, E. Luderer, R. Pazirandeh, U. Stettner, Nucl. Instr. and Meth. B 146 (1998) 131, Europhys. Lett. 47 (1999) 384;
G. Schiwietz, G. Xiao, E. Luderer, P.L. Grande, Nucl. Instr. Meth. B 164 (2000) 353.
[14] M. Caron, H. Rothard, M. Beuve, B. Gervais, Physica Scipta T 92 (2001) 281.

[15] G. Schiwietz, P.L. Grande, Nucl. Instr. and Meth. B 175–177 (2001) 125;
The casp code may be downloaded from http://www.hmi.de/people/schiwietz/casp.html.
[16] G. Schiwietz, D. Schneider, J.P. Biersack, N. Stolterfoht, D. Fink, A. Mattis, B. Skogvall, H. Altevogt, V. Montemayor, U. Stettner, Phys. Rev. Lett. 61 (1988) 2677.
[17] W. Schmidt, P. Müller, V. Brückner, F. Löffler, G. Saemann-Ischenko, W. Schubert, Phys. Rev. A 24 (1981) 2420.
[18] M. Krause, J. Phys. Chem. Ref. Data 8 (1979) 507.
[19] G. Schiwietz, P.L. Grande, Radiat. Effects Defects Solids 130–131 (1994) 137, and references therein.
[20] A. Koyama, H. Ishikawa, K. Maeda, Y. Sasa, O. Benka, M. Uda, Nucl. Instr. Meth. B 48 (1990) 608.